Electrochemical corrosion behavior and mechanical properties of Ti-Ag biomedical alloys obtained by two powder metallurgy processing routes

J.C Zambrano Carrullo[1], A. Dalmau Borrás[2], V. Amigó Borrás[1], J. Navarro-Laboulais[3], J.C Pereira Falcón[4]

[1] ITM, Institute of Materials Technology, Universitat Politècnica de València, camino de vera s/n, Valencia, 46022. Spain
[2] CIDETEC, Basque Research and Technology Alliance (BRTA), Pº. Miramón 196, 20014 Donostia-San Sebastián, Spain
[3] ISIRYM, Instituto Universitario de Seguridad Industrial, Radiofísica y Medioambiental, Universitat Politècnica de València, Camino de Vera s/n, 46022 Valencia, Spain
[4] LORTEK Technological Centre, Basque Research and Technology Alliance (BRTA), Arranomendia Kalea, 4A, Ordizia, 20240, Gipuzkoa, Spain
* Corresponding author: Tel.: +34 963 877 000 email: jenzamca@upv.es

Abstract: Titanium is frequently used as a biomaterial and the importance of Ti-Ag alloys has increased thanks to the antibacterial behavior of silver. In this study, Ti-Ag alloys (5, 10 and 15 wt.% Ag) were obtained by two different powder metallurgy routes: blended elemental (BE) and mechanical alloying (MA). The influence of the powder mixture methodology on both microstructure and electrochemical behavior was analyzed. Powders were compacted at 600 and 900 MPa, respectively, and sintered at high vacuum for 3 h at 950 °C. The obtained Ti-Ag alloys were microstructurally characterized by Scanning Electron Microscopy (SEM), Energy Dispersive X-Ray Spectroscopy (EDS) and X-Ray Diffraction (XRD), and mechanically tested by hardness and bending tests. Electrochemical tests were run using a three-electrode cell in an artificial Fusayama saliva solution. Open-Circuit Potential (OCP), polarization curves, potentiostatic tests and Electrochemical Impedance Spectroscopy (EIS) techniques were employed to evaluate the corrosion resistance of the studied Ti-Ag alloys. The initial characteristics of powders before sintering and after blend/alloying modified the electrochemical behavior of the Ti-Ag-sintered alloys and were determined. The samples obtained with the BE powders better resisted corrosion than the MA samples, and this behavior was directly related to the quantity and distribution of intermetallic Ti_2Ag. A large quantity of intermetallics present on both the edge and inside grains reduced the corrosion resistance of TiAg alloys.

Keywords: Ti-Ag; Powder Metallurgy; Mechanical Alloying; Corrosion; Biomaterial

1. Introduction

As titanium (Ti) presents specific properties, it is a widely used material in many fields, and is employed as a biomaterial for biomedical implants, for which the following are required: corrosion resistance, adequate mechanical properties where the modulus of elasticity needs to come as close as possible to the bone´s module, biocompatibility, osseointegration and easy manufacturing processes that allow the required parts to be obtained. As the properties of titanium alloys depend on both the chemical composition and the microstructure of Ti, alloys with the required properties are CP Ti, Ti-6Al-4V, Ti-Nb and Ti-Ta (Leyens and Peters, 2003). For instance, with the Ti alloys used in dental prosthesis, the alloy is exposed to different media when a part is placed in mouths, i.e. saliva, air, food, beverages, etc. This causes a reaction from the oxide layer that is naturally formed in Ti parts (Takada et al., 2001) because Ti spontaneously passivates, reacts with surrounding metals, and its behavior is limited, or poor, in the presence of fluorides at low pH (Prasad et al., 2015).

Several authors have studied binary Ti alloys for biomedical applications (Liu et al., 2017; Subramani et al., 2018; Takada et al., 2012), and prefer Beta-type alloys obtained by combining elements like Co, Cr, Fe, Mn or Pd in different proportions, where behavior against corrosion is similar to that presented by pure Ti. Alpha-type alloys have also been studied by combining Ti with elements like Cu and Ag. In the particular case of Ag, for a wt.% Ag over 20%, the alloy's corrosion resistance reduces because of the presence of intermetallic Ti_2Ag and/or Ti-Ag, which are preferentially formed on grain boundaries (Takada et al., 2001). Other authors have studied alloys with noble metals Ag, Au, Pd and Pt (10 wt.%) by focusing on the passive layers they form, and have found acceptable behavior against corrosion with 10% Ag (Hwang et al., 2015).

Silver as an alloying element is interesting because it presents antibacterial properties, such as Cu or Zn (Liu et al., 2014; Pina et al., 2016; Zhang et al., 2016, 2013), a similar cytotoxicity to pure Ti (Oh et al., 2005) and a slow ion release compared to Au. Aluminum displays good cytocompatibility, followed by Co-Cr castings and Ti-6Al-4V alloys (Liu et al., 2017). Several authors have observed alloys that have %Ag (up to 8% by weight) in corrosion studies in artificial saliva with fluoride ions, and have verified that Ag works by promoting the formation of a Ti oxide layer by passivating it (Oh et al., 2005; Shim et al., 2005). The Ti-Ag couple can form a galvanic cell promoting galvanic corrosion and thus, the oxidation of Ti, this has been reported by several authors (Mareci et al., 2017).

Takahashi *et al* (Takahashi et al., 2011) obtained different alloys by arc melting with Ag contents between 5 and 40 wt.%, to study their corrosion resistance in a solution of 0.9% NaCl and in lactic acid. They observed similar CP titanium behavior for % Ag below 17.5 wt.%. Ti_2Ag was present at a higher Ag%, which decreased corrosion resistance. Moreover, the presence of intermetallic Ti_2Ag increases the alloy's mechanical strength with a slow release of ions. Thus alloys with a maximum Ag content of 25 wt.% and a microstructure composed of α-Ti and Ti_2Ag on grain boundaries are recommended as they offer acceptable corrosion resistance (Takahashi et al., 2011, 2010, 2006).

Ag increases resistance to pure Ti corrosion by lowering the current density of potentiodynamic corrosion in artificial saliva, but this decreases when tested with fluoride ions. Other authors have reported an improvement when performing thermal oxidation surface treatment. As the *in vitro* cytotoxicity results showed they have cytocompatibility as CP Ti, they are considered suitable for dental applications (Liu et al., 2017; Zhang et al., 2012, 2011, 2009).

The massive transformation of β-Ti into α-Ti in such alloys is achieved by adding Ag, reinforcing the crystalline structure, and increasing the mechanical strength of alloys when they have a microstructure composed only of α-Ti to achieve similar corrosion resistance to that reported for CP Ti (Han et al., 2014; Hwang et al., 2015).

In the Ti-Ag alloys obtained by a conventional powder metallurgy route, the size of Ag particles (micrometric or nanometric) strongly influences the final percentage of Ag in alloys, which impacts their antibacterial characteristics. An increase in both hardness and mechanical resistance measured by compression tests with sintered samples has been verified, and antibacterial studies indicate that smaller Ag particle sizes enhance the antibacterial property, which is directly associated with the amount of intermetallic Ti_2Ag present and its distribution in the microstructure. By this manufacturing route, a higher percentage of intermetallics has been obtained than by other methods (Chen et al., 2017, 2016). Ti-Ag alloys achieved their best mechanical properties with 10 wt.% Ag in samples obtained by powder

Da Silva *et al* (da Silva Vieira Marques et al., 2015) gained bioactive coatings by plasma electrolytic oxidation (PEO) and adding Ag to obtain the required antibacterial effect. T. Yetim *et al* (Yetim, 2016) doped TiO_2 coatings with Ag on pure Ti, while W.F Cui (Cui et al., 2016) used Ag as an alloy element in Ti-Zr alloys, and corrosion resistance improved in both cases.

There is a wide spectrum of biomaterials and biomaterial surfaces designed to prevent postoperative infections in patients associated with the material. The decreased adhesion of bacteria would avoid their colonization, and a wide range of alternative methods are used, but employing a biomaterial with antibacterial properties would be better, or even ideal (Campoccia et al., 2013).

When implants are produced by the powder metallurgy route, the initial processing stage of powders can be carried out by either the blended elemental (BE) method or mechanical alloying (MA) of powders, which directly influences the distribution of Ag on the surface and in the microstructure obtained after compaction and sintering. Artificial saliva has been used by many authors to simulate the conditions under which an implant is subjected in mouths. The present study performs the electrolyte proposed by Miotto *et al* (Miotto et al., 2016)

The main objective of this work was to study the influence of both alternatives for initial powders processing by Ti-Ag alloys, BE and MA in the microstructure obtained after sintering, as well as their impact on mechanical properties and corrosion resistance. Another aim was to investigate whether Ag content directly influences such behavior.

2. Experimental Procedure

2.1 Alloy processing routes

Several Ti-Ag alloys were obtained with different Ag weight percentages (5, 10 and 15 wt.% Ag). Ti purity 99.7% (Atlantic Equipment Engineers Co, -325 mesh) was used, and the particle size of Ti varied from 11 to about 56 µm, with an average size of 30 µm. Silver powder with 99.99% purity (Alfa Aesar Co) and a particle size of 0.6-2 µm was selected. The particle size for the selected Ag particles was less than 10 µm, because some authors point out that with this particle size, Ag diffuse better due they present a greater surface area and have better packaging when cold pressed, contributing to the formation of necks between particles during early stage of sintering process and also the antibacterial behavior is improved with small particles size (Chen et al., 2016).

Two different processing routes to obtain the initial powders for the Ti-Ag alloys were used: (1) BE. The mixture of powders was prepared in an electrical tumbler mixer (Bioengineering Inversina 2L) for 20 minutes, where powders were mixed, but not alloyed, and the obtained particles were separated from one another; (2) the MA processing route. Powders were mechanically milled in a planetary mill (Retsch PM 400/2) at a rotation speed of 180 rpm for 52 minutes in steel jars, with metallic balls of chrome steel at a balls/powder weight ratio of 10:1 in an Ar atmosphere. Powder compaction was carried out in Instron hydraulic universal testing machine model 1343 at a press load of 600 MPa for the compaction of the BE samples and of 900 MPa for the MA samples. Higher compaction pressure was used because the hardness of the MA particles increased due to plastic deformation after milling, so reducing the obtained porosities is desirable. Sintering was carried out in a Carbolite HVT 15/75/450 tubular furnace at high vacuum (<10^{-4} mbars) with a sintering cycle of 950 °C for 3 h to obtain rectangular samples measuring 12x30x5 mm^3 with optimized sintering parameters from previous studies to ensure better alloy sintering (Amigó et al., 2019; Atay et al., 2018; Mohan et al., 2017).

2.2 Microstructural characterization

Samples were metallographically prepared wet-ground with 220, 500 and 1000 grit silicon carbide (SiC) papers and were polished until mirror-like finishing with diamond suspension (3 µm) and colloidal silica. The microstructure was observed under a Zeiss ULTRA55 field emission scanning electron microscope (FESEM) by an X-Max Oxford Instruments microanalysis system (20 µm² X-ray detector). A microanalysis was carried out by energy dispersive spectroscopy (EDS) for chemical composition quantification purposes. An optical microscope (model Nikon Eclipse LV100) was used to determine the porosity percentage by image analyses. Phase identification was confirmed by X-ray diffraction patterns with a Bruker D2 Phaser diffractometer and Cu Kα monochromatic radiation (λ= 0.15406 nm) within the 2θ range from 30º to 90º at 0.05°/min.

2.3 Mechanical characterization

To compare our different conditions, three-point bending tests were carried with the Universal testing machine Shimadzu autograph AG-X plus, 100 kN capacity, at a constant speed of 0.5 mm/min and a distance between supports of 25 mm. At least three samples were tested per condition. Hardness tests were run in a microhardness tester Shimadzu HMV-2 (300 g load) in at least eight areas to obtain a mean value with the corresponding standard deviation. Young´s modulus measures were taken by the ultrasonic method in a Karl Deutsh echograph model 1090, with longitudinal (DS6 PB-4-14) and transverse (YS 12 HB1) probes for longitudinal and transverse speed, respectively. Thickness was measured by a digital micrometer (RS components) before testing.

2.4 Electrochemical characterization

A potentiostat AUTOLAB PGSTAT204 performed the corrosion tests with a three-electrode cell configuration consisting of an Ag/AgCl (3M KCl) reference electrode, platinum wire as the counter electrode and a Ti alloy as the working electrode. All the potentials were provided according to the reference electrode. An artificial Fusayama's saliva solution was used as the electrolyte (NaCl:0.40 g/L, KCl: 0.40 g/L, $CaCl_2{\cdot}2H_2O$: 0.795 g/L, $NaH_2PO_4{\cdot}2H_2O$: 0.690 g/L, urea: 1 g/L, $Na_2S{\cdot}9H_2O$:0.005 g/L)(Miotto et al., 2016). Three samples per condition were used and were prepared until a mirror-like finishing was achieved. An ultrasonic bath with ethanol and acetone for 10 minutes was used for cleaning. Before taking measurements, cathodic cleaning was carried out by applying -1.1 V for 300 s. The OCP vs. time was recorded for 1800 s. The Electrochemical Impedance Spectroscopy (EIS) technique was followed within the 100 kHz – 5 mHz frequency range with a sinusoidal amplitude wave of 0.01 V on E_{ocp}. Potentiodynamic polarization curves were carried out by swiping the potential from -1 V to 3 V at the 2 mV/s scan rate. Electrochemical parameters were obtained by Tafel slope extrapolation and impedances data were acquired by the Zview 3.5f software by fitting equivalent circuits. Chronoamperometric tests were carried out at 1 V (passivation potential) for 5 min with a 0.01 s time interval for data acquisition in the previously prepared samples.

3. Results

3.1 Initial characterization of the material

The theoretical density was calculated based on the percentage by weight and the specific density of each element and using the inverse rule of mixtures (German, 2005, 1998), as shown in the equation 1, with the known theoretical density values of titanium (4.507 g/cm^3) and silver (10.50 g/cm^3)

$$\rho_{Alloy} = \frac{100}{\frac{\%wt.Ti}{\rho_{Ti}} + \frac{\%wt.Ag}{\rho_{Ag}}} \qquad \text{Eq. (1)}$$

The **green density** (g/cm^3) in the green parts was calculated dividing the mass of the material (g) by the volume of the piece (prism, cm^3) after cold compaction/pressing of the samples. The mean values and their deviation were calculated from measurements made on three samples of each alloy under study. They are compiled now in **Table 1** for MA TiAg alloys for reference. The values for BE are not available. The relative density (g/cm^3) is determined using Archimedes method which is determined accordingly to ASTM C373 (ASTM, 2018).

The density values obtained indicate that mechanical alloying samples are more porous compared to those obtained by elemental mixing, which is an expected result in this type of process. The density obtained by the Archimedes method shows the open porosities and the porosities (%) reported in the table which have been obtained by image processing show the closed porosities, this percentage of porosity was considered acceptable and barely impacted alloys' behavior.

Table 1. Previous characterization of alloys through different densities and porosity

Sample	Ag content (wt.%)	Theoretical Density (g/cm^3)	Green Density (g/cm^3)	Relative Density (%)	Porosity by Archimedes (%)	Porosity by image (%)
Blended elemental (BE)	5	4.639	-	94.78 ± 0.36	5.22 ± 0.36	2.4 ± 0.5
	10	4.780	-	95.66 ± 0.34	4.34 ± 0.34	3.0 ± 1.0
	15	4.948	-	96.92 ± 0.09	3.08 ± 0.09	2.4 ± 0.6
Mechanical alloying (MA)	5	4.639	3.734 ± 0.01	90.06 ± 0.08	9.94 ± 0.08	4.0 ± 1.0
	10	4.780	3.886 ± 0.01	91.16 ± 0.10	8.04 ± 0.10	3.0 ± 1.0
	15	4.948	4.026 ± 0.01	90.23 ± 0.09	9.77 ± 0.09	5.0 ± 1.0

The morphology of the initial particles of the pure metals for both powders are seen in the micrograph of **Figure 1a** and **Figure 1b**, obtained by being placed on a carbon band and observed by SEM. The mechanical alloyed powders are observed in **Figure 1c**, **1d** and **1e**, where Ag (white) is inside Ti particles (gray). We can see that large-sized Ag clusters formed, and the homogeneity of samples increased with 10 and 15 wt.% Ag (**Figure 1d** and **1e**). To observe these powders, they were previously placed in resin and prepared metallographically to show the cross-section in SEM.

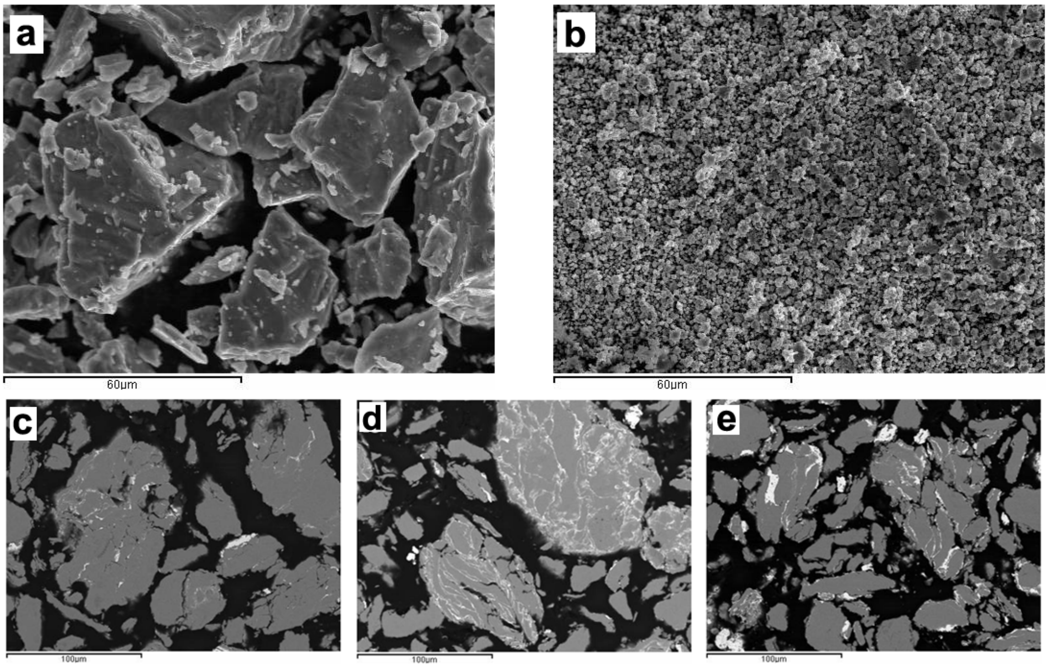

Figure 1. SEM images in Secondary Electron (SE) mode of starting powders before sintering: **a)** Ti powder and **b)** Ag powder. **c), d)** and **e)** SEM of the cross-section of Ti powders with 5, 10 and 15 wt.% Ag after mechanical alloying.

3.2 Microstructural characterization

Figure 2 shows the micrographs of the alloys by means of FESEM with EDS, and the indication of the spectrum points for the chemical compositions of all the alloys. The presence of two phases was observed and verified. For the samples obtained by BE (**Figure 2a**, **2b** and **2c**) and MA (**Figure 2d**, **2e** and **2f**), there were α-Ti grains (light gray phase) with the corresponding percentage per Ag weight in solution (approx. 5, 10 and 15 wt.% Ag) and the presence of intermetallic Ti_2Ag (white phase) (with approx. 50 wt.% Ag) on grain boundaries.

The samples obtained by BE contained Ag in the solid solution in the Ti matrix. Precipitation of the intermetallic Ti_2Ag on the grain boundary for 15%wt. had a bigger proportion of Ag. For the MA samples, a higher percentage of intermetallic Ti_2Ag was observed on grain boundaries and increased with Ag content, as shown in **Figure 2**. For the semi-quantitative measurements of the chemical composition carried out by EDS in the white phase, Ag content was around 50 wt.% and came close to the theoretical 53% that corresponded to the chemical composition of intermetallic Ti_2Ag. **Table 2** compiled the chemical composition obtained from sum spectrums measured for each sample in an area of 1800 μm^2 and summarizes the values measured for the chemical composition of the spectrums indicated in the samples presented in **Figure 2**.

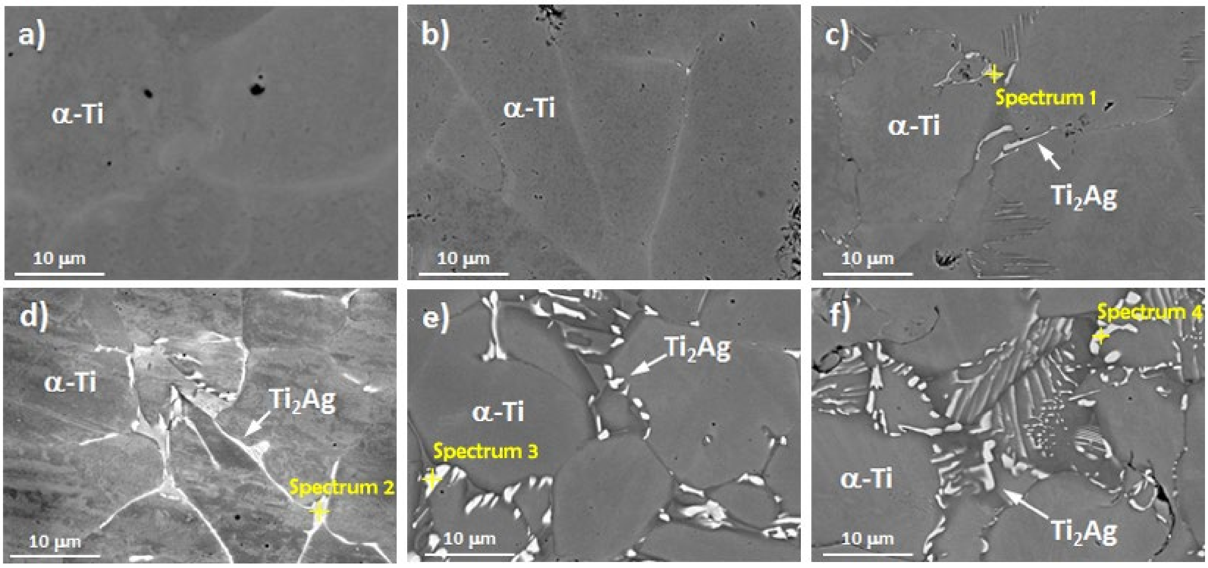

Figure 2. FESEM micrographs in backscattered electron (BSE) mode of samples obtained from the blended elemental powders with 5, 10 and 15 wt.% Ag (**a, b** and **c**) and the mechanical alloyed samples with 5, 10 and 15 wt.% Ag (**d, e** and **f**)

Table 2. Chemical composition for the spectrums indicated in **Figure 2**

Sample	**Sum Spectrum (wt.%)**		**Point**	**(wt.%)**	
	Ti	**Ag**		**Ti**	**Ag**
Ti-5Ag_BE	94.60	5.40	-	-	-
Ti-10Ag_BE	88.90	11.10	-	-	-
Ti-15Ag_BE	85.10	14.90	Spectrum 1	50.80	49.20
Ti-5Ag_MA	94.84	5.16	Spectrum 2	51.30	48.70
Ti-10Ag_MA	90.90	9.10	Spectrum 3	50.70	49.30
Ti-15Ag_MA	84.70	15.30	Spectrum 4	51.10	48.90

Figure 3 shows the content of the two main phases, obtained by the image processing of micrographs. By analyzing the area for each phase, we can see almost 8% of intermetallic Ti_2Ag for the Ti-15Ag_MA alloy obtained by MA, and almost 2% for the Ti-15Ag_BE alloy obtained by BE.

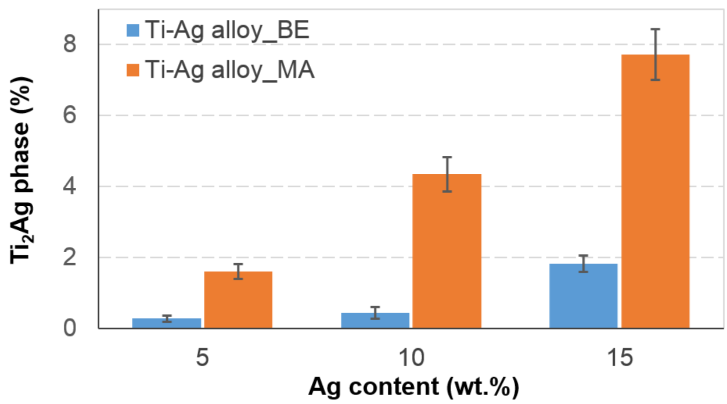

Figure 3. Comparison of the amount of the Ti_2Ag phase measured for both processing routes according to the Ag weight contents in Ti-Ag alloys

The X-Ray diffraction patterns (**Figure 4**) show the peaks corresponding to the α-Ti phase and intermetallic Ti_2Ag. Intermetallic Ti_2Ag was identified only in the MA samples with 15 wt.% Ag. Several authors point out that at least four peaks of Ti_2Ag overlap Ti peaks (Chen et al., 2016; Han et al., 2014), including the peak of the plane of greater intensity (013) of Ti_2Ag in 2θ, which equals 38.07 and is superimposed on the plane (002) of α-Ti. The planes (110) and (006) in 2θ equal 43.38 and 45.95, respectively. However, their intensity is very low and determining their presence may be difficult. We expected to find these peaks for a higher Ag content in the alloy, but we were unable to verify the presence of intermetallic Ti_2Ag using a scan step of 0.05 °/min.

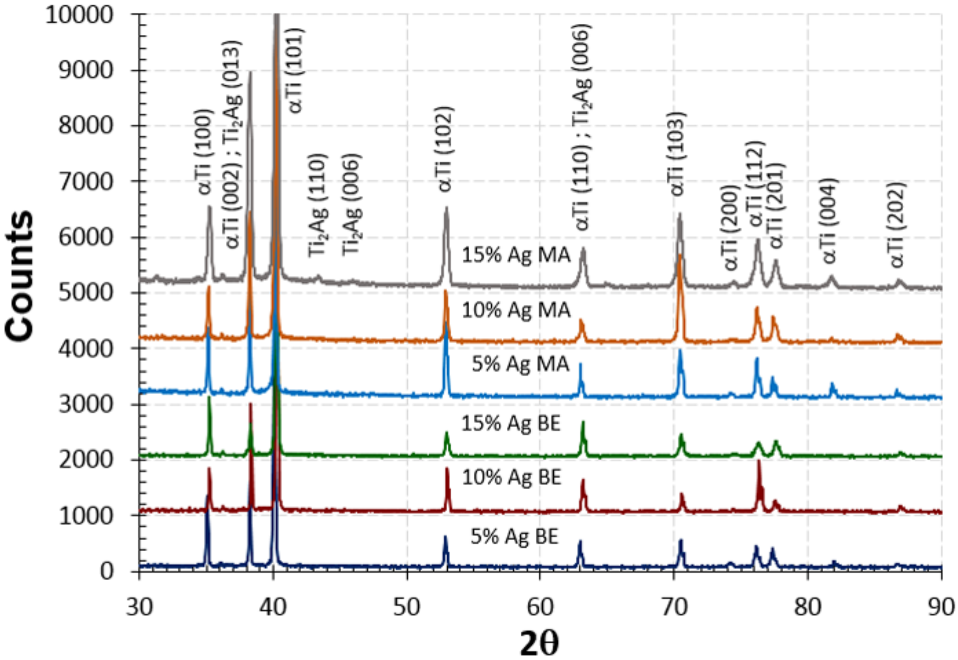

Figure 4. X-Ray diffractograms of the blended elemental (BE) and mechanical alloying (MA) samples

3.3 *Mechanical characterization*

The results of the hardness measurements and the mechanical properties obtained in the three-point bending tests are shown in **Table 3.** Previous studies report that the presence of Ag increases the alloy's hardness compared to pure Ti obtained by casting (Chen et al., 2016; Szaraniec and Goryczka, 2017). The measured hardness of our samples ranged from 222 to 281 HV for the BE samples, and between 286 and 394 HV for the MA samples. Previously reported samples obtained by powder metallurgy processes ranged from 300 to 400 HV, which was as expected. For the bending tests run with the BE samples, greater mechanical strength (in terms of Flexural strength) than those obtained with the MA samples was observed. The presence of intermetallics on the grain boundary and in the colonies in the latter contributed to embrittlement, which caused plastic deformation to considerably diminish which, in turn, influenced the maximum obtained resistance. The modulus of elasticity was similar for both BE and MA samples, with values coming close to those for CP Ti.

Table 3. Mechanical properties obtained in the studied Ti-Ag alloys.

Sample	Ag content (wt.%)	Hardness (HV0.3)	Flexural strength (MPa)	Deformation at break (%)	E (GPa)
CP Ti (PM)	0	327 ± 37	1308 ± 110	16 ± 4	108 ± 2
Blended elemental (BE)	5	222 ± 22	1224 ± 40	6 ± 1	100 ± 2
	10	270 ± 21	1464 ± 74	8 ± 1	102 ± 3
	15	281 ± 27	1427 ± 160	5 ± 2	103 ± 3
Mechanical alloying (MA)	5	394 ± 34	457 ± 28	3 ± 0.5	91 ± 10
	10	286 ± 37	462 ± 42	2 ± 0.2	105 ± 3
	15	331 ± 62	444± 31	2 ± 0.2	98 ± 1

3.4 Electrochemical characterization

The potentiodynamic polarization curves of the different Ti-Ag alloys and CP Ti are shown in **Figure 5**. Three domains appeared on the curve of pure Ti (black line): the cathodic domain from -1 V to -0.5 V; the transition between the cathodic and anodic domains (from -0.5 V to 0 V); the passive domain until the end of testing, characterized by a TiO_2 oxide layer forming that limited the current flow. No transpassive domain was noted. The Ti-Ag alloys behaved as follows:

- BE alloys (red lines): shifted slightly to the more anodic potentials and had a transpassive domain
- MA alloys (blue lines): moved to more cathodic potentials and current density increased by 1 order of magnitude

An anodic peak was noted at around 0.10 V for the BE samples of the Ti-Ag alloys in bigger Ag proportions, which corresponded to the pure Ag dissolution. This behavior was observed by Takada *et al* in Ti-Ag alloys with a bigger quantity of Ag (Takada et al., 2001).

The results of the corrosion parameters are shown in **Table 4.** , which summarizes the open-circuit potential (E_{ocp}) and the average of the last 300 recorded values, where slope E(V)-t(s) was constant. The corrosion potential (E_{corr}), corrosion current density (i_{corr}), anodic and cathodic Tafel constants (b_a, b_c) and polarization resistance (R_p) results were obtained from the potentiodynamic polarization curves by the Tafel extrapolation method. A non linear adjustment was made with the Wolfram Mathematica 11.3 program using the Buttler-Volmer equation (Equation 2)(Landolt, n.d.) near the corrosion potential in a 50mV window to obtain the electrochemical parameters, where: anodic and cathode Tafel's coefficients (b_{an} and b_{cat}) are defined by Equations 3 and 4; α is the charge transfer coefficient, n is the number of electrons; F is the Faraday constant; η is the overpotential.

$$i(\eta) = i_{corr}\left(\exp\left(\frac{n\,\alpha}{R\,T}\eta\right) - \exp\left(-\frac{n(1-\alpha)}{R\,T}\eta\right)\right) \quad \text{Eq. (2)}$$

$$b_{an} = \frac{\ln 10 \cdot R\,T}{n\,\alpha\,F} \quad \text{Eq. (3)}$$

$$b_{cat} = -\frac{\ln 10 \cdot R\,T}{n(1-\alpha)\,F} \quad \text{Eq. (4)}$$

The MA Ti-Ag alloy presented higher corrosion current density values and a more cathodic value for E_{corr} (negative) than the CP Ti and BE samples. However, the BE Ti-Ag alloys exhibited similar corrosion current densities and more anodic values of E_{corr} than CP Ti, which indicates improved corrosion resistance. The cathodic and anodic Tafel slopes were lower for the MA samples than for the BE ones. The obtained polarization resistance values corresponded to the expected values, and the BE samples were like those of CP Ti, but were higher than those of the MA samples.

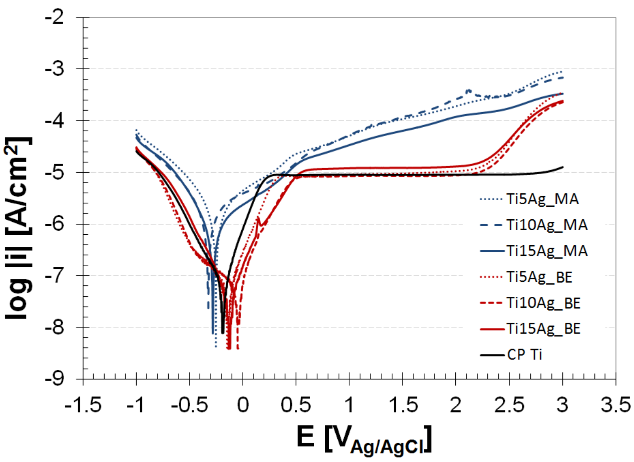

Figure 5. Potentiodynamic polarization curves of Ti-Ag alloys in artificial Fusayama saliva solution with blended elemental (BE) and mechanical alloying (MA) powders and CP Ti

Table 4. Electrochemical parameters obtained from the potentiodynamic polarization curves in the studied Ti-Ag alloys.

Sample	Ag content (wt.%)	E_{ocp} (V)	E_{corr} (V)	i_{corr} (μA/cm^2)	b_{cat} (V/dec)	b_{an} (V/dec)	R_p (kΩ. cm^2)
CP Ti (PM)	0	-0.24±0.10	-0.19±0.07	0.03±0.002	0.12±0.020	0.11±0.140	7.25E5±0.6
Blended elemental (BE)	5	-0.24±0.10	-0.11±0.03	0.02±0.001	0.12±0.003	0.10±0.002	9.77E5±0.2
	10	-0.25±0.04	-0.14±0.14	0.02±0.002	0.14±0.020	0.09±0.009	9.91E5±1.0
	15	-0.20±0.02	-0.10±0.01	0.01±0.003	0.13±0.006	0.09±0.003	17.85E5±4.0
Mechanical alloying (MA)	5	-0.03±0.03	-0.31±0.09	0.43±0.059	0.11±0.001	0.12±0.001	0.59E5±0.1
	10	-0.06±0.01	-0.39±0.10	0.41±0.112	0.11±0.001	0.12±0.001	0.62E5±0.2
	15	-0.07±0.02	-0.27±0.08	0.33±0.181	0.10±0.001	0.12±0.001	0.87E5±0.5

The Nyquist diagrams of the EIS experiments are shown in **Figure 6** for all the studied Ti-Ag alloys and CP Ti. Nyquist spectra were similarly semicircular arc in shape, which is characteristic of passive metals. The Ti-5Ag_BE sample behaved like CP Ti, and Ti-10Ag_BE and Ti-15Ag_BE behaved better because a longer semicircle length is associated with higher R_p resistance. The MA samples exhibited different behavior as the diameter of the semicircle considerably decreased, indicating that its resistance to corrosion is much lower and its behavior does not depend directly on the silver content. In the Bode diagrams (**Figure 7**), similar behavior took place for the CP Ti and BE Ti-Ag samples, mainly for 5 and 10 wt.% Ag, with a phase angle close to 90°, which indicates capacitive behavior over a wide frequency range., Both the impedance modulus and the phase angle in the intermediate frequencies area diminished for the MA samples, which indicates less corrosion resistance.

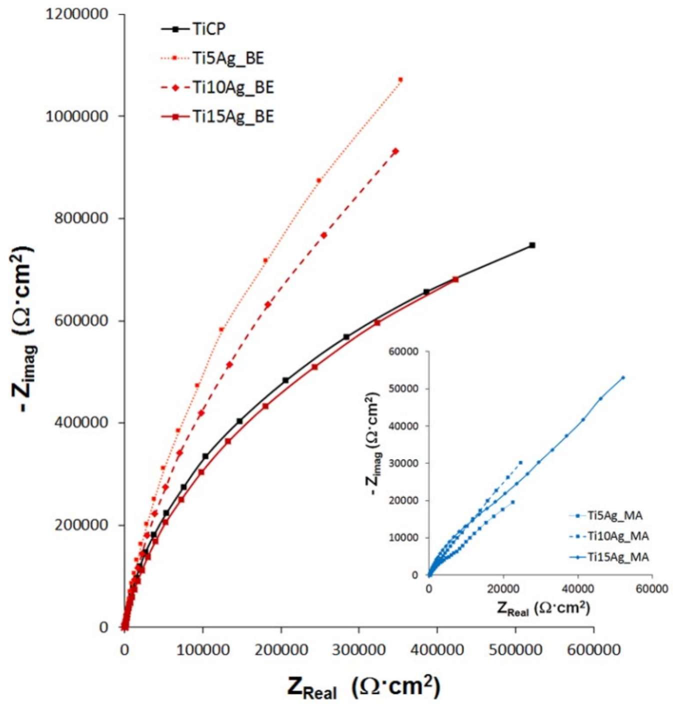

Figure 6. Nyquist diagrams of the CP Ti and Ti-Ag alloys with 5, 10 and 15 wt.% Ag by blended elemental (BE) and mechanical alloying (MA)

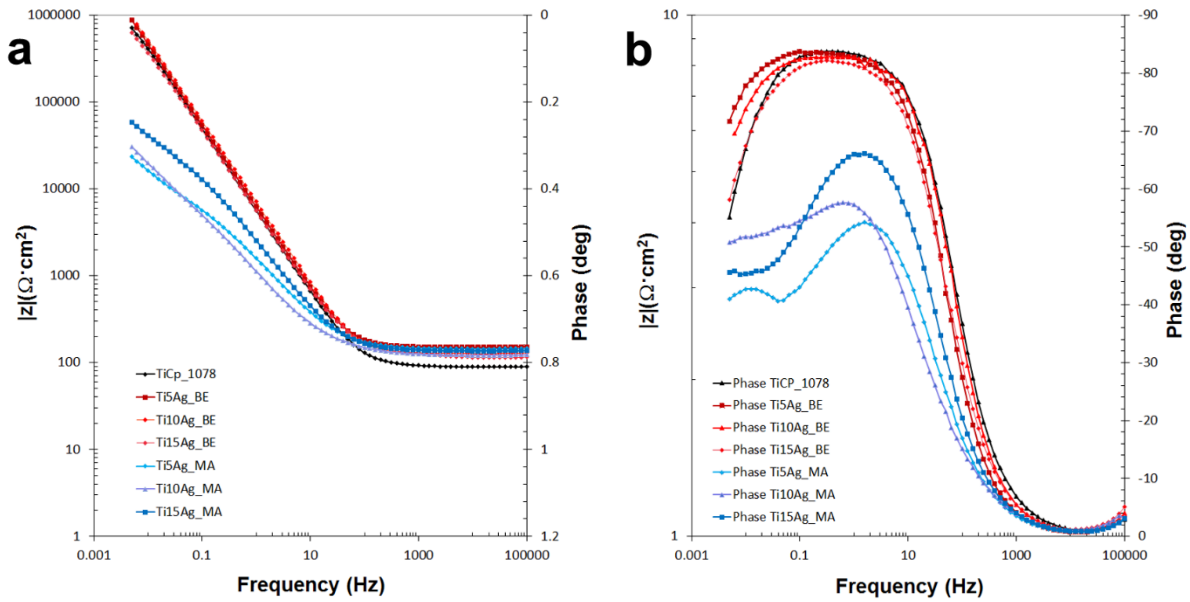

Figure 7. Bode diagrams of the CP Ti and Ti-Ag alloys with 5, 10 and 15 wt.% Ag by blended elemental (BE) and mechanical alloying (MA)

The results were fitted with an equivalent that simulated the electrical double layer in those series with a passive porous layer (**Figure 8**) by the ZView software (version 3.5f), where a constant phase element (CPE) was introduced to replace the capacitor after considering non ideal behavior with R_s, R_{ct}, R_{film}, R_p, CPE_{dl} and CPE_{film}, like solution resistance, charge transfer resistance, film resistance, polarization resistance, double-layer CPE and film's CPE. This has been used by other authors for CP Ti and Ti alloys, and represents the equivalent circuit that best fits the corrosion mechanism composed of metal/compact inner layer/porous outer layer/electrolyte with the corresponding interfaces (Bolat et al., 2013; da Silva Vieira Marques et al., 2015; Dalmau et al., 2015, 2013; González and Mirza-Rosca, 1999; Pan et al., 1996; Ureña et al., 2018, 2017; Xie et al., 2015; Zhang et al., 2011). Another variable employed to describe passive layers, n_{dl}, is the coefficient of CPEdl, n_{film}, which is the exponential coefficient of CPE_{film}, while interface CPE_{dl} and the electrolyte and transfer charge resistance are related to C_{dl} (Eq. 4), $CPEf_{ilm}$, and R_s, R_{ct} and R_{film} are related to C_{film} (Eq. 5), as described by Dalmau *et al* (Dalmau et al., 2013). All these parameters appear in **Table 5.** .

$$C_{dl} = \left(\frac{CPE_{dl}}{(R_s{}^{-1}+R_{ct}{}^{-1})^{1-n_{dl}}}\right)^{1/n_{dl}} \quad \text{(Eq. 4)}$$

$$C_{film} = \left(\frac{CPE_{film}}{((R_s+R_{ct})^{-1}+R_{film}{}^{-1})^{1-n_{film}}}\right)^{1/n_{film}} \quad \text{(Eq. 5)}$$

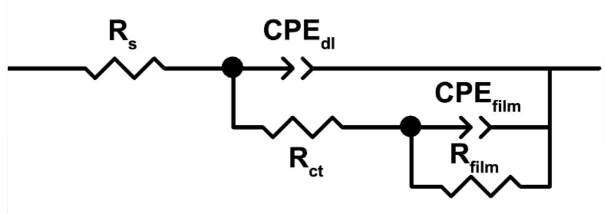

Figure 8. Equivalent circuit fitted for the CP Ti and Ti-Ag alloys for a double porous oxide layer

Table 5. Electrochemical parameters obtained by the Electrochemical Impedance Spectroscopy (EIS) technique in the studied Ti-Ag alloys

Samples	R_s (Ω.cm²)	CPE_{dl} (μF/cm²)	n_{dl}	R_{ct} (kΩ.cm²)	C_{dl} (μF/cm²)	CPE_{film} (μF/cm²)	n_{film}	R_{film} (kΩ.cm²)	C_{film} (μF/cm²)
CP Ti (PM)	89	21	0.94	0.13	14.93	9	0.93	1380	6

Ti-5Ag_BE	150	24	0.93	0.24	16.38	4	0.93	3903	3
Ti-10Ag_BE	126	22	0.93	0.17	13.87	3	0.94	2901	2
Ti-15Ag_BE	116	12	0.93	0.06	7.25	20	0.91	1412	12
Ti-5Ag_MA	143	156	0.73	9.22	40.22	379	0.70	63	614
Ti-10Ag_MA	122	254	0.70	31.53	59.47	286	0.90	79	352
Ti-15Ag_MA	136	87	0.81	27.94	31.54	143	0.63	400	305

The values obtained from R_s were similar in all cases, and charge transfer resistance R_{ct} was much lower than film R_{film} resistance, which many authors have related to the internal oxide layer as it is much more protective than the outer layer (Dalmau et al., 2015; Xie et al., 2015). Coefficients n_{dl} and n_{film} corresponded to the outer and the inner layer, respectively, and came close to 0.90 for the BE samples. Their values were lower for the MA samples, which indicates better capacitive behavior for BE (Xie et al., 2015). The C_{dl} and C_{film} values were lower for the BE samples with higher resistance R_p values, which implies better corrosion behavior (Dalmau et al., 2015). The obtained settings had an χ^2 of an order of 10^{-4}, which denotes that the used equivalent circuits are representative of the formed oxide layers.

In the first few seconds of the chronoamperometric tests, and as shown in **Figure 9**, the decrease in current density over time, due to oxide layer formation, i_{pp} (passivation current density) and charge Q (obtained as an area under the curve) (Dalmau et al., 2015), which describe the dissolution and dissolved cation rates, were greater for the MA samples than the BE ones and CP Ti (see **Table 6**). These actions correspond to those obtained in previous electrochemical tests and point out that intermetallics has a marked influence on cation activity on surfaces.

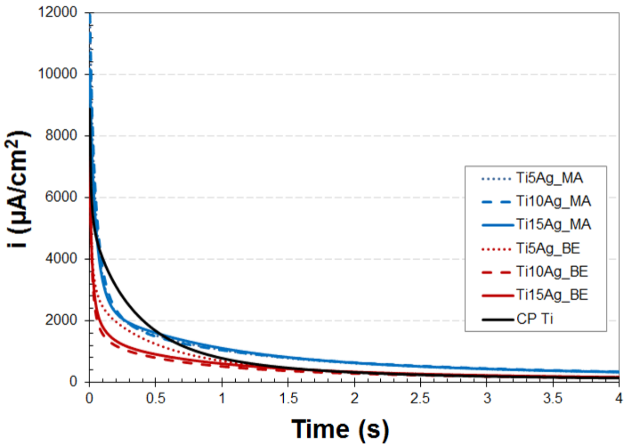

Figure 9. Potentiostatic curves of the CP Ti and Ti-Ag alloys for the first seconds of tests

Table 6. Electrochemical parameters obtained in the potentiostatic tests in the studied Ti-Ag alloys

Samples	i_{pp} (μA/cm²)	Q (mC.cm²)
CP Ti (PM)	1.57 ± 0.05	0.26 ± 0.11
Ti-5Ag_BE	1.59 ± 0.17	0.28 ± 0.20
Ti-10Ag_BE	2.44 ± 0.74	0.17 ± 0.08
Ti-15Ag_BE	1.85 ± 0.11	0.26 ± 0.003
Ti-5Ag_MA	11.18 ± 1.48	0.61 ± 0.46
Ti-10Ag_MA	10.14 ± 1.59	0.88 ± 0.60
Ti-15Ag_MA	28.98 ± 18.89	0.55 ± 0.11

4 Discussion

According to the phase diagram of the Ti-Ag alloy (Murray, 1987), for Ag values below 6 wt.%, Ag was completely dissolved in the Ti and solid solution α-Ti formed. Intermetallic Ti_2Ag precipitation was expected for higher Ag values. When some authors obtained the Ti-Ag alloy by casting or arc melting, solidification was faster and considered to be in non-equilibrium when α-Ti was obtained only for Ag percentages up to 20 wt.% (Chen et al., 2017, 2016; Szaraniec and Goryczka, 2017; Takada et al., 2001; Takahashi et al., 2011, 2010, 2006). For parts obtained by powder metallurgy, intermetallic Ti_2Ag precipitation occurred at wt.% Ag between 3 and 8 wt.% Ag on grain boundaries. These results have been reported by different authors with powder mechanical alloys (Chen et al., 2017; Szaraniec and Goryczka, 2017), which coincides with the quantity of intermetallic Ti_2Ag herein found in the samples obtained by both routes (BE and MA).

When powders are obtained by the BE process, Ti and Ag particles are mixed with a uniform distribution separately in the alloy before sintering. When powder is processed by MA, particles are repeatedly flattened, welded in successive cold fractures and rewelded, which confers the microstructure greater homogeneity after sintering (Lu and Lai, 1995; Suryanarayana, 2001). In this study, the initial powder MA processing stage promoted intermetallic Ti_2Ag precipitation, which can be attributed to Ag particulates being embedded during titanium presintering. Other authors have verified that small Ag particle sizes contribute to the diffusion mechanism (Chen et al., 2016).

The hardness of Ti-Ag alloys was greater than that of CP Ti alloys when produced by casting. Increased hardness was caused mainly by solid solution hardening, which reinforced the α-Ti matrix with Ag atoms and intermetallic precipitation (Ti_2Ag). Hardness became higher due to the concentration of alloy elements, which usually exhibit high strength and low ductility by laminated Ti_2Ag and their ability to reinforce by dispersion in the matrix (Chen et al., 2017, 2016; Han et al., 2014; Oh et al., 2005; Takahashi et al., 2009, 2002). In our case, the CP Ti obtained by PM had hardness values like those of the BE samples of Ti-Ag because the presence of intermetallic Ti_2Ag was verified only in the samples with 15 wt.% Ag. The presence of Ti_2Ag was verified for all the MA samples (5, 10 and 15 wt.% Ag), with no clear influence of the percentage of Ag. We found that the presence of intermetallics directly influence the mechanical behavior of the Ti-Ag samples by decreasing their ductility or plastic deformation capacity, and by increasing hardness and improving mechanical resistance. The parts obtained by powder metallurgy were affected by the shape of porosity, which made the material more fragile by plastic deformation in the powders obtained by both BE and MA. Finally, hardening could be due to oxygen content, which must be confirmed.

Tensile tests on powder metallurgical products are complex and, since they are more brittle than casting products, they may not achieve the real properties of the material. Using bend testing and in particular three-point flexural test, both stresses (traction and compression) are combined, allowing the determination of the mechanical and plastic properties of powder metallurgical materials in a simpler and, above all, precise way, which allows comparatively simple comparison of the properties of the powder metallurgical materials. In Ti-Ag alloys obtained by both powder metallurgy routes, the mechanical properties depend directly on the obtained microstructure when α-Ti and intermetallic Ti_2Ag are present in small amounts (maximum 2%). The obtained properties were considered acceptable for their high resistance and ductility, and also due to the higher percentages of Ag (35 wt.% Ag). Some authors have obtained microstructures with another intermetallics, such as Ti-Ag, and mechanical resistance reduced, while the modulus of elasticity increased (Szaraniec and Goryczka, 2017). Hence intermetallic Ti_2Ag precipitation was required to improve the mechanical properties of the Ti-Ag alloys obtained by the powder metallurgy route. However, it has been verified that if the amount of intermetallics present exceeds 2%, its hardness increases, and its mechanical resistance decreases, which occurred with the MA samples.

Two different electrochemical behaviors were observed between Ti-Ag alloys by MA and BE. On the one hand, the MA Ti-Ag alloys catalyzed the cathodic reaction and exhibited higher current densities and lower polarization resistances. On the other hand, the BE Ti-Ag alloys presented a higher potential and corrosion resistance. These differences in corrosion behavior of both fabrication processes can be attributed to the distribution of Ag in the microstructure of Ti-Ag alloys. Several authors have found in the samples they obtained by casting or powder metallurgy that Ag improved corrosion resistance, provided that the obtained microstructure was α-Ti (Chen et al., 2017, 2016; Han et al., 2014; Takahashi et al., 2010, 2006). However, ductility reduces and weakens with large quantities of Ti_2Ag, as we found herein, and is present on both the edge and grain of Ti (Shim et al., 2005). Thus, for the same Ag content, the electrochemical response differs depending on the initial powder preparation conditions before pressing and sintering because this direct influences the obtained microstructure.

Similar behavior between the BE and CP Ti samples was observed in the potentiodynamic tests on the polarization curves, with passive layers forming up to 2.3V for the BE Ti-Ag alloys. In these samples, the corrosion resistance of the Ag dissolved in Ti improved. With the MA samples, the presence of the intermetallics reduced corrosion resistance independently of the influence of Ag content because of the preferential dissolution in the areas close to the intermetallics, as verified by several authors in different media (Takada et al., 2001; Takahashi et al., 2010, 2006). The amount of Ag in samples improved corrosion resistance in the BE samples by increasing polarization resistance R_p and decreasing corrosion current density (i_{corr}) compared to CP Ti (see **Figure 10**). The corrosion resistance of the samples obtained from the initial processed powders was worse.

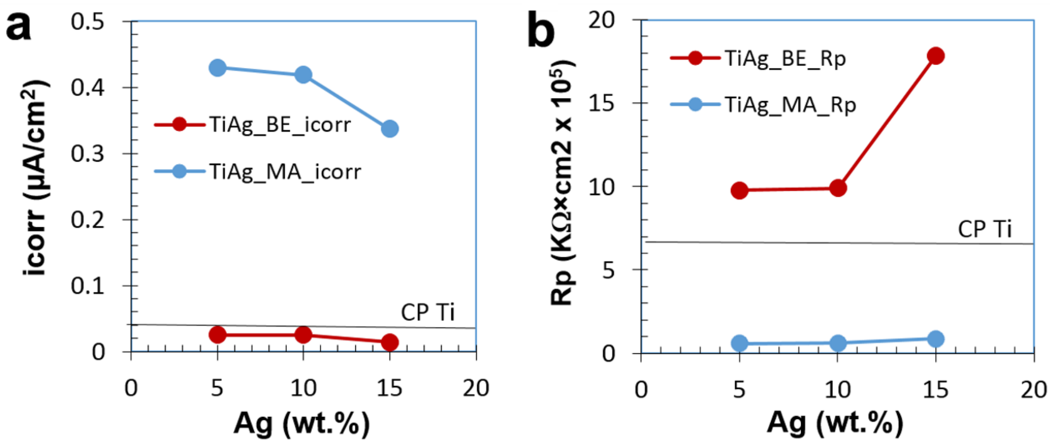

Figure 10. Influence of Ag content on **a)** icorr and **b)** R_p on the studied Ti-Ag alloys compared to CP Ti

With the current-time data obtained from the chronoamperometric tests, a double logarithmic representation was made to deduce the relation between these two quantities. From a theoretical point of view, a functional relation of type shown in the equation exists:

$$I(t) \propto t^{-n} \qquad \text{(Eq. 6)}$$

If electrode processes are controlled by diffusion n = ½, the expression is reduced to the Cottrell equation. When n = 1, the electrode's behavior is purely capacitive. A logarithmic double representation was made to evaluate this exponent and the result is shown in **Figure 11**.

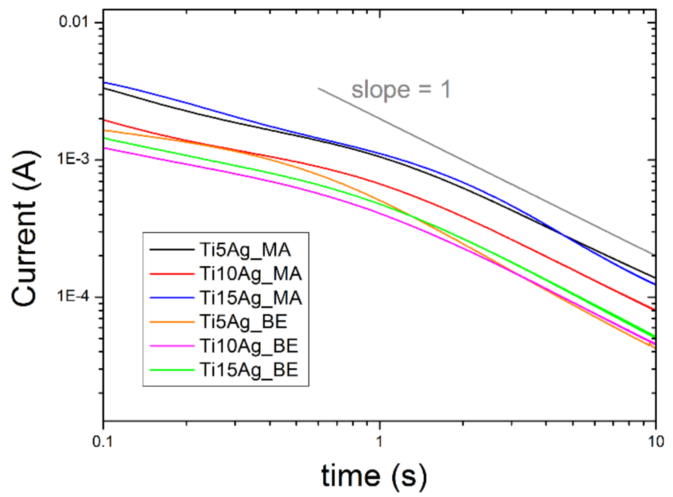

Figure 11. Corrosion current vs. time in a double logarithmic representation

The unit slope line acts only as a visualization aid. We found that beyond 4-5 s, the current's behavior was exclusively capacitive. Below 1 s, the slope of curves was less than and close to ½. The lines above 5 s had a greater intercept for the MA samples than for the BE ones. This is consistent with the results obtained from EIS, where the CPE exponents for MA were in the order of 0.75 and those of BE came close to unity. We obtained a bigger electrode surface for higher roughness values, which implies higher values in the intercepts in the linear sections of **Figure 11**. The chronoamperometric data showed similar behavior, where the heterogeneity of the surface of the material prepared by MA was greater than when prepared by BE. So, for times shorter than 1 s, we expected Cottrell-type behavior. **Figure 12** represents current *versus* $1/\sqrt{t}$.

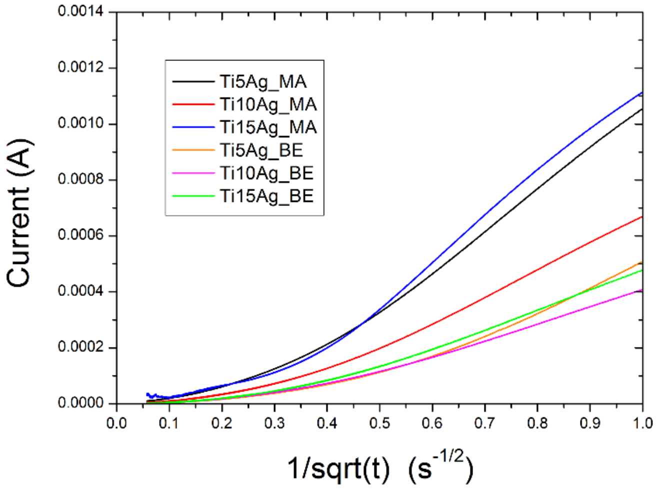

Figure 12. Corrosion current vs. $1/\sqrt{t}$ in a double logarithmic representation

The section of these curves for times between 0.5 and 1.0 was linear, which indicates that the diffusive control regime was fully developed. The section that deviated from the linear behavior for t <0.5 can be associated with not only limited diffusion phenomena on the passive layer, but also with ohmic fall phenomena due to the solution's high resistance, as confirmed by the EIS measurements.

The influence of the initial powder conditions before pressing and sintering can be seen in both mechanical and electrochemical properties. Using this type of alloys with initial BE processing is recommended because it has a considerable Ag content in samples, which is desirable from an antibacterial point of view (Chen et al., 2017; da Silva Vieira Marques et al., 2015). Moreover, properties are like CP Ti, which has been used to date as a biomaterial.

5 Conclusions

The following conclusions can be drawn from studying the influence of the powder mixture or alloying method on the manufacturing process of Ti-Ag biomedical alloys by the powder metallurgy route:

- From a microstructural point of view, Ti-Ag alloys formed by α-Ti and the intermetallic compound Ti_2Ag were obtained by a conventional press and sintering route. The samples obtained with BE had lower percentages of Ti_2Ag and porosities
- The maximum resistance measured in the bending of BE samples was greater compared to MA samples, with higher mechanical resistance values due to their fragility and the reduced plastic deformation capacity, generated mainly by intermetallic Ti_2Ag being present in the microstructure
- Corrosion resistance improved with the Ag content of BE samples compared to pure Ti (CP Ti) in the samples obtained by MA, whose corrosion resistance was lower *versus* BE samples and CP Ti due to the presence of intermetallics, which dissolves preferentially in these types of alloys in corrosive environments.

Acknowledgements

The authors wish to thank the Generalitat Valenciana for support through PROMETEO 2016/040. Alba Dalmau acknowledges the Generalitat Valenciana for her grant (APOSTD/2017/051), the European Commission via FEDER funds to purchase equipment for research purposes in ISIRYM and the Ministry of Science, Innovation and Universities for the project RTI2018-097810-B-I00. Finally, they thank the Microscopy Service at Universitat Politècnica de València in Spain.

Data Availability

The raw/processed data required to reproduce these findings cannot be shared at this time due to technical or time limitations.

References

Amigó, A., Vicente, A., Afonso, C., Amigó, V., 2019. Mechanical Properties and the Microstructure of β Ti-35Nb-10Ta-xFe Alloys Obtained by Powder Metallurgy for Biomedical Applications. Metals (Basel). 9, 76. https://doi.org/10.3390/met9010076

ASTM, 2018. ASTM C373 - 18 Standard Test Methods for Determination of Water Absorption and Associated Properties by Vacuum Method for Pressed Ceramic Tiles and Glass Tiles and Boil Method for Extruded Ceramic Tiles and Non-tile Fired Ceramic Whiteware Products.

Atay, H.Y., Rodriguez, M.H., Mata, A.A., Escuder, A. V, Borrás, V.A., 2018. Investigations of Ti Binary Alloys Manufactured by Powder Metallurgy for Biomaterial Applications. Acta Phys. Pol. A. 134.

Bolat, G., Mareci, D., Chelariu, R., Izquierdo, J., González, S., Souto, R.M., 2013. Investigation of the electrochemical behaviour of TiMo alloys in simulated physiological solutions. Electrochim. Acta 113, 470–480. https://doi.org/https://doi.org/10.1016/j.electacta.2013.09.116

Campoccia, D., Montanaro, L., Arciola, C.R., 2013. A review of the biomaterials technologies for infection-resistant surfaces. Biomaterials 34, 8533–8554. https://doi.org/https://doi.org/10.1016/j.biomaterials.2013.07.089

Chen, M., Yang, L., Zhang, L., Han, Y., Lu, Z., Qin, G., Zhang, E., 2017. Effect of nano/micro-Ag compound particles on the bio-corrosion, antibacterial properties and cell biocompatibility of Ti-Ag alloys. Mater. Sci. Eng. C 75, 906–917. https://doi.org/https://doi.org/10.1016/j.msec.2017.02.142

Chen, M., Zhang, E., Zhang, L., 2016. Microstructure, mechanical properties, bio-corrosion properties and antibacterial properties of Ti–Ag sintered alloys. Mater. Sci. Eng. C 62, 350–360. https://doi.org/https://doi.org/10.1016/j.msec.2016.01.081

Cui, W.F., Liu, N., Qin, G.W., 2016. Microstructures, mechanical properties and corrosion resistance of the ZrxTi (Ag) alloys for dental implant application. Mater. Chem. Phys. 176, 161–166. https://doi.org/https://doi.org/10.1016/j.matchemphys.2016.04.009

da Silva Vieira Marques, I., Barão, V.A.R., da Cruz, N.C., Yuan, J.C.-C., Mesquita, M.F., Ricomini-Filho, A.P., Sukotjo, C., Mathew, M.T., 2015. Electrochemical behavior of bioactive coatings on cp-Ti surface for dental application. Corros. Sci. 100, 133–146. https://doi.org/https://doi.org/10.1016/j.corsci.2015.07.019

Dalmau, A., Pina, V.G., Devesa, F., Amigó, V., Muñoz, A.I., 2015. Electrochemical behavior of near-beta titanium biomedical alloys in phosphate buffer saline solution. Mater. Sci. Eng. C 48, 55–62. https://doi.org/https://doi.org/10.1016/j.msec.2014.11.036

Dalmau, A., Pina, V.G., Devesa, F., Amigó, V., Muñoz, A.I., 2013. Influence of fabrication process on electrochemical and surface properties of Ti–6Al–4V alloy for medical applications. Electrochim. Acta 95, 102–111. https://doi.org/https://doi.org/10.1016/j.electacta.2013.01.155

German, R., 2005. A - Z of Powder Metallurgy, Metal powders technology series. Elsevier Science.

German, R.M., 1998. Powder Metallurgy of Iron and Steel. Wiley.

González, J.E.G., Mirza-Rosca, J.C., 1999. Study of the corrosion behavior of titanium and some of its alloys for biomedical and dental implant applications. J. Electroanal. Chem. 471, 109–115. https://doi.org/https://doi.org/10.1016/S0022-0728(99)00260-0

Han, M.-K., Hwang, M.-J., Won, D.-H., Kim, Y.-S., Song, H.-J., Park, Y.-J., 2014. Massive Transformation in Titanium-Silver Alloys and Its Effect on Their Mechanical Properties and Corrosion Behavior. Materials (Basel). 7, 6194–6206. https://doi.org/10.3390/ma7096194

Hwang, M.J., Park, E.J., Moon, W.J., Song, H.J., Park, Y.J., 2015. Characterization of passive layers formed on Ti-10wt% (Ag, Au, Pd, or Pt) binary alloys and their effects on galvanic corrosion. Corros. Sci. 96, 152–159. https://doi.org/10.1016/j.corsci.2015.04.007

Landolt, D., n.d. Corrosion and Surface Chemistry of Metals. CRC Press.

Leyens, C., Peters, M., 2003. Titanium and titanium alloys: fundamentals and applications. John Wiley & Sons. https://doi.org/10.1002/3527602119.

Liu, J., Li, F., Liu, C., Wang, H., Ren, B., Yang, K., Zhang, E., 2014. Effect of Cu content on the antibacterial activity of titanium–copper sintered alloys. Mater. Sci. Eng. C 35, 392–400. https://doi.org/https://doi.org/10.1016/j.msec.2013.11.028

Liu, X., Chen, S., Tsoi, J.K.H., Matinlinna, J.P., 2017. Binary titanium alloys as dental implant materials—a review. Regen. Biomater. 4, 315–323. https://doi.org/10.1093/rb/rbx027

Lu, L., Lai, M.O., 1995. Formation of new materials in the solid state by mechanical alloying. Mater. Des. 16, 33–39. https://doi.org/https://doi.org/10.1016/0261-3069(95)00005-J

Mareci, D., Bocanu, C., Aelenei, N., Nemtoi, G., 2017. Galvanic Corrosion Between Ti/Ti6Al4V and Various Dental Alloys. Eurasian Chem. J. 6, 221. https://doi.org/10.18321/ectj615

Miotto, L.N., Fais, L.M.G., Ribeiro, A.L.R., Vaz, L.G., 2016. Surface properties of Ti-35Nb-7Zr-5Ta: Effects of long-term immersion in artificial saliva and fluoride solution. J. Prosthet. Dent. 116, 102–111. https://doi.org/https://doi.org/10.1016/j.prosdent.2015.10.024

Mohan, P., Elshalakany, A.B., Osman, T.A., Amigo, V., Mohamed, A., 2017. Effect of Fe content, sintering temperature and powder processing on the microstructure, fracture and mechanical behaviours of Ti-Mo-Zr-Fe alloys. J. Alloys Compd. 729, 1215–1225. https://doi.org/https://doi.org/10.1016/j.jallcom.2017.09.255

Murray, J.L., 1987. Phase diagrams of binary titanium alloys. ASM Int. 340–345.

Oh, K.-T., Shim, H.-M., Kim, K.-N., 2005. Properties of titanium–silver alloys for dental application. J. Biomed. Mater. Res. Part B Appl. Biomater. 74B, 649–658. https://doi.org/10.1002/jbm.b.30259

Pan, J., Thierry, D., Leygraf, C., 1996. Electrochemical impedance spectroscopy study of the passive oxide film on titanium for implant application. Electrochim. Acta 41, 1143–1153. https://doi.org/https://doi.org/10.1016/0013-4686(95)00465-3

Pina, V.G., Amigó, V., Muñoz, A.I., 2016. Microstructural, electrochemical and tribo-electrochemical characterisation of titanium-copper biomedical alloys. Corros. Sci. 109, 115–125. https://doi.org/https://doi.org/10.1016/j.corsci.2016.02.014

Prasad, S., Ehrensberger, M., Gibson, M.P., Kim, H., Monaco, E.A., 2015. Biomaterial properties of titanium in dentistry. J. Oral Biosci. 57, 192–199. https://doi.org/https://doi.org/10.1016/j.job.2015.08.001

Shim, H.-M., Oh, K.-T., Woo, J.-Y., Hwang, C.-J., Kim, K.-N., 2005. Corrosion resistance of titanium–silver alloys in an artificial saliva containing fluoride ions. J. Biomed. Mater. Res. Part B Appl. Biomater. 73B, 252–259. https://doi.org/10.1002/jbm.b.30206

Subramani, K., Mathew, R.T., Pachauri, P., 2018. Chapter 6 - Titanium surface modification techniques for dental implants—From microscale to nanoscale, in: Subramani, K., Ahmed, W. (Eds.), Emerging Nanotechnologies in Dentistry (Second Edition), Micro and Nano Technologies. William Andrew Publishing, pp. 99–124. https://doi.org/https://doi.org/10.1016/B978-0-12-812291-4.00006-6

Suryanarayana, C., 2001. Mechanical alloying and milling. Prog. Mater. Sci. 46, 1–184. https://doi.org/https://doi.org/10.1016/S0079-6425(99)00010-9

Szaraniec, B., Goryczka, T., 2017. Structure and properties of Ti-Ag alloys produced by powder metallurgy. J. Alloys Compd. 709, 464–472. https://doi.org/https://doi.org/10.1016/j.jallcom.2017.03.155

Takada, Y., Nakajima, H., Okuno, O., Okabe, T., 2001. Microstructure and Corrosion Behavior of Binary Titanium Alloys with Beta-stabilizing Elements. Dent. Mater. J. 20, 34–52. https://doi.org/10.4012/dmj.20.34

Takada, Y., Takahashi, M., Kikuchi, M., 2012. The Development of Binary Titanium Alloys with the Aim of Dental Applications, in: Sasaki, K., Suzuki, O., Takahashi, N. (Eds.), Interface Oral Health Science 2011. Springer Japan, Tokyo, pp. 66–71.

Takahashi, M., Kikuchi, M., Hatori, K., Orii, Y., Sasaki, K., Takada, Y., 2009. Calcium Phosphate Formation on Ti-Ag Alloys in Simulated Body Fluid. J. Biomech. Sci. Eng. 4, 318–325. https://doi.org/10.1299/jbse.4.318

Takahashi, M., Kikuchi, M., Takada, Y., 2011. Corrosion behavior of Ti-Ag alloys used in dentistry in lactic acid solution. Met. Mater. Int. 17, 175–179. https://doi.org/10.1007/s12540-011-0224-y

Takahashi, M., Kikuchi, M., Takada, Y., Okabe, T., Okuno, O., 2006. Electrochemical Behavior of Cast Ti-Ag Alloys. Dent. Mater. J. 25, 516–523. https://doi.org/10.4012/dmj.25.516

Takahashi, M., Kikuchi, M., Takada, Y., Okuno, O., 2010. Corrosion Resistance of Dental Ti-Ag Alloys in NaCl Solution. Mater. Trans. advpub, 1002150998. https://doi.org/10.2320/matertrans.M2009355

Takahashi, M., Kikuchi, M., Takada, Y., Okuno, O., 2002. Mechanical Properties and Microstructures of Dental Cast Ti-Ag and Ti-Cu Alloys. Dent. Mater. J. 21, 270–280. https://doi.org/10.4012/dmj.21.270

Ureña, J., Gordo, E., Ruiz-Navas, E., Vilaboa, N., Saldaña, L., Jiménez-Morales, A., 2017. Electrochemical comparative study on corrosion behavior of conventional and powder metallurgy titanium alloys in physiological conditions. Met. Powder Rep. 72, 118–123. https://doi.org/https://doi.org/10.1016/j.mprp.2016.04.003

Ureña, J., Tsipas, S., Pinto, A.M., Toptan, F., Gordo, E., Jiménez-Morales, A., 2018. Corrosion and tribocorrosion behaviour of β-type Ti-Nb and Ti-Mo surfaces designed by diffusion treatments for biomedical applications. Corros. Sci. 140, 51–60. https://doi.org/https://doi.org/10.1016/j.corsci.2018.06.024

Xie, F., He, Xueming, Lv, Y., Wu, M., He, Xinbo, Qu, X., 2015. Selective laser sintered porous Ti–(4–10)Mo alloys for biomedical applications: Structural characteristics, mechanical properties and corrosion behaviour. Corros. Sci. 95, 117–124. https://doi.org/https://doi.org/10.1016/j.corsci.2015.03.005

Yetim, T., 2016. Corrosion Behavior of Ag-doped TiO2 Coatings on Commercially Pure Titanium in Simulated Body Fluid Solution. J. Bionic Eng. 13, 397–405. https://doi.org/10.1016/S1672-6529(16)60311-6

Zhang, B.B., Qiu, K.J., Wang, B.L., Li, L., Zheng, Y.F., 2012. Surface Characterization and Cell Response of Binary Ti-Ag Alloys with CP Ti as Material Control. J. Mater. Sci. Technol. 28, 779–784. https://doi.org/https://doi.org/10.1016/S1005-0302(12)60130-3

Zhang, B.B., Wang, B.L., Li, L., Zheng, Y.F., 2011. Corrosion behavior of Ti–5Ag alloy with and without thermal oxidation in artificial saliva solution. Dent. Mater. 27, 214–220. https://doi.org/10.1016/J.DENTAL.2010.10.005

Zhang, B.B., Zheng, Y.F., Liu, Y., 2009. Effect of Ag on the corrosion behavior of Ti–Ag alloys in artificial saliva solutions. Dent. Mater. 25, 672–677. https://doi.org/https://doi.org/10.1016/j.dental.2008.10.016

Zhang, E., Li, F., Wang, H., Liu, J., Wang, C., Li, M., Yang, K., 2013. A new antibacterial titanium–copper sintered alloy: Preparation and antibacterial property. Mater. Sci. Eng. C 33, 4280–4287. https://doi.org/https://doi.org/10.1016/j.msec.2013.06.016

Zhang, E., Wang, X., Chen, M., Hou, B., 2016. Effect of the existing form of Cu element on the mechanical properties, bio-corrosion and antibacterial properties of Ti-Cu alloys for biomedical application. Mater. Sci. Eng. C 69, 1210–1221. https://doi.org/https://doi.org/10.1016/j.msec.2016.08.033